

Segmentation of Ink and Parchment in Dead Sea Scroll Fragments

Berat Kurar-Barakat^{1*} and Nachum Dershowitz¹

¹*Blavatnik School of Computer Science, Tel Aviv University, Tel Aviv, Israel.

*Corresponding author(s). E-mail(s): berat@tauex.tau.ac.il;

Contributing authors: nachum@tau.ac.il;

Abstract

The discovery of the Dead Sea Scrolls over sixty years ago is widely regarded as one of the greatest archaeological breakthroughs in modern history. Recent study of the scrolls presents ongoing computational challenges, including determining the provenance of fragments, clustering fragments based on their degree of similarity, and pairing fragments that originate from the same manuscript—all tasks that require focusing on individual letter and fragment shapes. This paper presents a computational method for segmenting ink and parchment regions in multispectral images of Dead Sea Scroll fragments. Using the newly developed Qumran Segmentation Dataset (QSD) consisting of 20 fragments, we apply multispectral thresholding to isolate ink and parchment regions based on their unique spectral signatures. To refine segmentation accuracy, we introduce an energy minimization technique that leverages ink contours, which are more distinguishable from the background and less noisy than inner ink regions. Experimental results demonstrate that this Multispectral Thresholding and Energy Minimization (MTEM) method achieves significant improvements over traditional binarization approaches like Otsu and Sauvola in parchment segmentation and is successful at delineating ink borders, in distinction from holes and background regions.

Keywords: Ink segmentation, parchment segmentation, multispectral thresholding, energy minimization

1 Introduction

The discovery of the Dead Sea Scrolls (DSS) in the 1940s and 1950s is one of the greatest archaeological breakthroughs in modern history. These ancient texts were written or copied mainly between the 2nd century BCE and the 2nd century CE. In the early days of DSS studies, scholars with direct access sometimes performed physical repairs that caused damage [1], or rearranged photographic prints manually by cutting and taping fragments [2]. Both practices lacked precision and occasionally obscured important information. To ensure their preservation and accessibility,

the Israel Antiquities Authority (IAA) launched a project to photograph the DSS using high-resolution multispectral imaging [3] and made them publicly accessible through the Leon Levy Dead Sea Scrolls Digital Library [4]. These images (Figure 1) significantly reduce the need to physically handle the scrolls, thereby minimizing the risk of deterioration from environmental exposure.

The availability of high-resolution digital images has shifted scholarly practices from traditional to digital humanities, where digital tools are used to address humanities research questions. As a result, traditional scholarly editions are

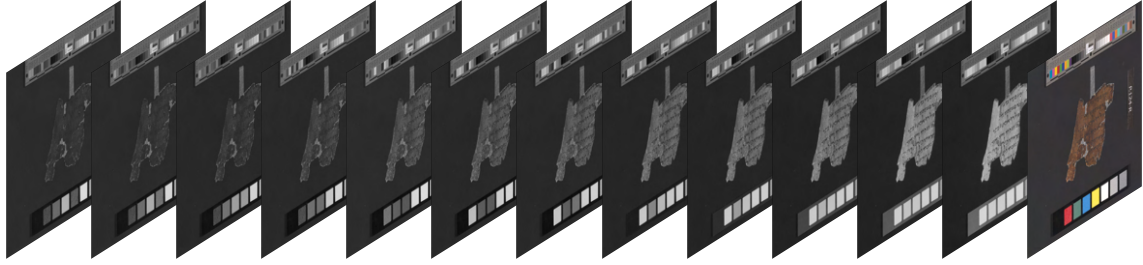


Fig. 1 Multispectral imaging of a DSS fragment at different wavelengths. The images represent bands 1 to 12 from left to right, followed by the color image on the far right. The first seven images are in the visible light spectrum, and the remaining five are in near-infrared



Fig. 2 Ink and parchment segmentation in a Dead Sea Scroll (DSS) fragment using Multispectral Thresholding and Energy Minimization (MTEM)

evolving into digital scholarly editions. A scholarly edition is a critical representation of historical documents, either visually (through images) or abstractly (through transcriptions) [5]. Critical representation involves scholarly interpretation and contextualization of documents, aiming either to reconstruct a lost ‘Urtext’ or to realize the author’s intended version of a contaminated text [6]. This includes enriching textual scholarship [6] by transcription, translation [7, 8], augmenting with variants [9], and even identifying individual scribes [10]. Digital scholarly editions are scholarly editions that are guided by a digital paradigm in their method and practice for reconstruction by paleography, codicology and shape matching [1, 11–16].

Moreover, the availability of these images has enabled advances in computational humanities, where algorithms are developed to address humanities research problems, including transcription-to-image alignment [17], paleography [18–22], codicology [23–25], handwriting recognition [17, 26], fragment matching [27, 28], and character restoration [29].

Effective utilization of these digital and computational methods depends heavily on segmenting DSS images into homogeneous regions. Segmentation allows scholars to move, superimpose, and toggle regions for visual analysis. It is also vital for computational tasks such as letter-level paleographical analysis, aligning OCR outputs with spatial positions of letters, matching fragment shapes across old and new photos, and analyzing handwriting similarity and parchment texture separately.

Typically, scholars perform segmentation manually using image editing tools [1, 11–16]. In contrast, computer scientists often apply thresholding to segment rice paper [28], parchment [23, 24], and ink regions [18, 21, 22]. Some approaches avoid explicit segmentation altogether [17], while others employ state of the art deep learning models, which are annotation costly, to segment ink [19, 20, 30] and parchment [27]. Surrogate classes have also been introduced to facilitate training without manual annotation [31].

Segmenting DSS images poses several challenges. As with many historical manuscripts, the DSS suffer from degradation due to aging: ink fades and parchment darkens over time [32]. Moreover, the choice of black background in the digitization process, while optimal for reducing light reflection and stabilizing imaging, creates severe low-contrast issues between ink, background, and holes.

We present the first attempt to segment DSS images into three distinct regions: parchment, ink, and background (Figure 2). A particularly challenging subclass of background regions consists of holes in the parchment. These holes resemble ink in both shape and size and are surrounded by parchment, making them difficult to distinguish

from true ink regions. Although parchment usually has higher contrast and is easier to detect, it often includes embedded ink and holes. Therefore, simple strategies such as closing low contrast regions can misclassify holes as parchment and misassign ink near parchment edges to the background.

We propose *Multispectral Thresholding with Energy Minimization (MTEM)* for segmenting DSS images into parchment, ink, and background. The method begins by applying multispectral thresholding to identify the parchment region. Although ink and background often share similar intensity values, we exploit a key insight: the contour regions around ink strokes exhibit higher reflectance due to the thin layer of ink blending with the parchment. These contours are extracted via thresholding and serve as seed regions for ink. We then apply energy minimization to propagate these seeds allowing ink contours to recover full ink regions from non-parchment areas, while the parchment mask guides the separation of background regions from non-parchment areas.

Our method exhaustively assigns each pixel in a DSS fragment image to one of the three classes: parchment, ink, or background. It does not rely on morphological operations or edge detection, and it avoids assumptions about component size. We created the Qumran Segmentation Dataset (QSD), which contains full pixel-level annotations for parchment, ink, and background across a selected subset of DSS fragment images. The dataset is publicly available at <https://www.cs.tau.ac.il/~berat> and is intended to support reproducibility and facilitate comparison of segmentation methods.

The structure of the paper is as follows: Section 2 reviews related work; Section 3 introduces the Qumran Segmentation Dataset (QSD); Section 4 presents the proposed MTEM segmentation method; Section 5 describes the experimental setup; and Section 6 reports the quantitative and qualitative results and analysis.

2 Related work

Image binarization is typically performed as a preprocessing step in document analysis systems to enable or improve subsequent tasks such as optical character recognition (OCR). The goal of binarization is to classify each pixel in the input

image as either foreground or background. Otsu's method [33] is one of the most widely used global thresholding techniques. This unsupervised, non-parametric approach selects a global threshold based on the grayscale histogram of the image, without requiring prior information. While effective for images with uniform backgrounds, Otsu's method often fails on historical manuscripts, which tend to have degraded and uneven backgrounds. Local adaptive thresholding methods address this limitation by operating on small image patches [34, 35] or detected edges [36, 37]. However, their performance depends on the size of the local window or detected edges, which can lead to suboptimal results when stroke widths vary significantly across the image. Wolf and Doermann [38] proposed a probabilistic Markov Random Field (MRF) model that incorporates spatial relationships between pixels to preserve stroke connectivity but this time increasing sensitivity to the noise variance. Gatos et al. [39] later introduced a parameter-free adaptive method based on estimated character height, which performs well on text regions but is less effective on non-textual regions.

Recently, deep learning based binarization methods have shown notable improvements over traditional techniques by addressing multiple challenges simultaneously. Vo et al. [40] used a hierarchical network to combine low and high level features for robust text prediction. Zhao et al. [41] applied conditional GANs to merge multi-scale predictions. He and Schomaker [42] proposed an iterative enhancement framework to recover clean document representations. Kang et al. [43] introduced modular U-Nets to handle limited training data, and He and Schomaker [44] combined enhancement and binarization tasks in a chained-cascade network. Despite their success, these methods are limited to grayscale images and focus only on segmenting dark text from light backgrounds, relying on local patches with limited spatial context.

While most binarization techniques have been developed for grayscale images, multispectral imaging has gained traction for enhancing the readability of historical documents. It is particularly useful for revealing faint or obscured writings. For instance, in studies of ancient Hebrew ostraca, near-infrared wavelengths have been shown to improve contrast between ink and

background [45, 46]. In the case of palimpsests, early approaches used dimensionality reduction methods such as Independent Component Analysis (ICA) [47] and Principal Component Analysis (PCA) [48, 49]. More recently, generative neural networks have been applied to uncover hidden layers of text [50].

Multispectral imaging has also been widely used for segmenting dark text regions from lighter backgrounds. A common strategy is to model spectral differences between foreground and background using a Gaussian Mixture Model (GMM), and to enforce spatial consistency and stroke connectivity using Markov Random Fields (MRFs) with Iterated Conditional Modes (ICM) optimization [51, 52]. Some approaches estimate the spectral signature of handwritten text by binarizing visible spectral bands, followed by the Adaptive Coherence Estimator (ACE) for pixel-level foreground detection [53]. This approach has been extended by integrating ACE-based target detection with a GrabCut framework, resulting in improved segmentation quality [54]. Further refinement has been achieved through preprocessing, such as applying median filtering to suppress background variation before GMM clustering [55]. More recently, Fully Convolutional Networks (FCNs) trained on manually annotated multispectral images have outperformed earlier methods in foreground and background prediction [53, 55].

Image binarization and multispectral segmentation methods in historical document analysis typically aim to extract low-contrast text from high-contrast backgrounds while preserving stroke continuity. However, the requirements for DSS segmentation differ substantially. Rather than enforcing connectivity, DSS segmentation must preserve broken strokes as they appear, in order to retain the integrity of the original ink regions. Moreover, not all ink regions correspond to coherent strokes; some may be smudges or ink drops from adjacent areas. In addition to the challenge of separating ink from the low-contrast, non-uniform parchment, segmentation is further complicated by holes and background regions, which often exhibit no contrast difference from ink, making accurate delineation particularly difficult.

Binarization approaches tailored to DSS fragments often leverage multispectral imaging. Lavee

[31] trained a binary Support Vector Machine (SVM) on grayscale intensities across multiple wavelengths, using Sauvola binarization for initial labels. Zarai et al. [56] extended this by incorporating historical scans from the 1950s, taken against a white background, into the SVM training process. However, neither approach aims to separate ink from the background; instead, they focus solely on distinguishing ink from parchment.

Dhali et al. [30] proposed BiNet, an end-to-end binarization method for DSS fragments based on the U-Net architecture [57]. BiNet focuses on segmenting ink as the foreground, grouping all other materials, including parchment and background, into a single background class. While it successfully separates ink from the background, it does not distinguish parchment from the background. Although this supervised approach significantly outperforms unsupervised methods, it requires 4–8 hours of manual annotation per fragment by expert paleographers.

3 Qumran Segmentation Dataset (QSD)

The Qumran Segmentation Dataset (QSD) was created to support reproducibility and enable the evaluation and comparison of methods for segmenting ink, parchment, and background regions in DSS fragment images. Segmenting these regions enables a more detailed investigation of the scrolls’ textual content and material properties, laying the foundation for further computational analysis and scholarly research. This section outlines the digitization process of the scrolls, describes the dataset’s composition, the preprocessing applied to prepare the data, and details the data annotation process.

3.1 Digitization of the Dead Sea Scrolls

The IAA initiated a digitization project in 2011 aimed at preserving the Dead Sea Scrolls and increasing access to them. Full-color and infrared images are publicly available online through the Leon Levy Dead Sea Scrolls Digital Library [58]. This allows scholars and the general public to explore them, while at the same time addressing deterioration caused by environmental factors and improper handling.

During digitization, each fragment is stabilized using rice tissue paper to limit movement and is photographed in 12 wavelengths (Figure 1), as listed in Table 1.

Table 1 Multispectral wavelengths used for photographing each fragment, comprising seven wavelengths in the visible light spectrum and five in the near-infrared spectrum

Visible light wavelengths	Near-infrared wavelengths
445nm – Royal Blue	IR706nm
475nm – Long Blue	IR728nm
499nm – Cyan	IR772nm
540nm – Green	IR858nm
595nm – Amber	IR924nm
638nm – Red	
656nm – Deep Red	

All of the visible light wavelengths are then combined to create a full-color digital image (Figure 3). All images have a resolution of 7216×5412 pixels, regardless of the actual size of the fragments. In the digital library, the full-color image and the last band image are accessible to everyone, while the other exposures are available to researchers upon request.

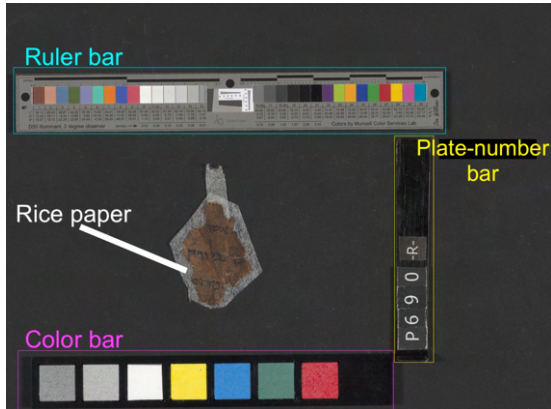


Fig. 3 An example IAA full-color image showing the color bar, ruler bar, plate-number bar, and the rice paper used to stabilize the fragment

Although a blue background would have made it easier to computationally isolate fragments from their background by providing high contrast with the parchment and ink, black was chosen to minimize light reflection [59]. A two-part water-based urethane coating [60] with low reflectance over a

wide wavelength range was applied to a stone surface to prevent background light from affecting the captured images. IAA images typically contain three types of bars: a color bar, a ruler bar, and a plate-number bar. The positions of these bars are identical in all band images of a given fragment but vary across different fragments and this variation causes challenges in detecting the fragment in the image (Figure 3).

3.2 Dataset composition and preprocessing

The QSD consists of images for 20 fragments. For each fragment, the dataset includes a full-resolution, full-color 8-bit JPEG image; a full-resolution, first-band 16-bit TIFF image; a full-resolution, last-band 16-bit TIFF image; and a normalized, full-resolution last-band 8-bit JPEG image (Figure 4). The full-color and normalized last-band JPEG images are provided for ease of use and visualization, while the 16-bit TIFF images are intended for quantitative analysis. Each image was processed by cropping the rectangular region containing the fragment and rice paper, while excluding the color bar, ruler bar, and plate-number bar [61]. This preprocessing reduces the dataset size, since a single full-color image exceeds 5 MB and a single band image exceeds 70 MB, making the dataset more manageable and ensuring that the focus remains on segmentation rather than detection.

The full-color images are 8-bit, have three channels, and are saved in JPEG format, with pixel values ranging from 0 to 255 for each channel. The normalized last-band images are also 8-bit, single-channel, and saved in JPEG format, with pixel values ranging from 0 to 255. In contrast, the multispectral first-band and last-band images are 16-bit, single-channel TIFF files, with pixel values ranging from 0 to 65535.

3.2.1 Characteristics of first-band and last-band images

Typically, raw 16-bit first-band and last-band images appear dark because the pixel values cover a wide range, with most concentrated in a narrow portion. After normalization, we can see the ink is minimally visible in the first-band and maximally visible in the last-band (Figure 22). This

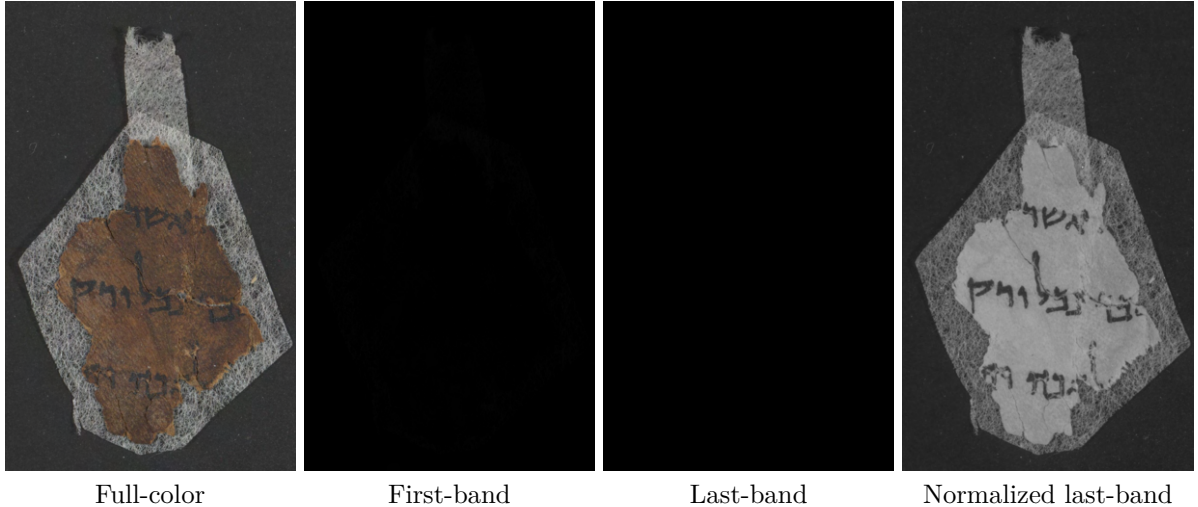


Fig. 4 The QSD dataset includes full-color, first-band, last-band, and normalized last-band images of each fragment, cropped to exclude the color bar, ruler bar, and plate-number bar. The first-band and last-band images appear dark due to the narrow range of pixel values in the 16-bit format. The full-color image and the normalized last-band image are useful for qualitative evaluation

is because the parchment has low reflectivity in the blue band and high reflectivity in the near-infrared bands, while the ink remains consistently low in reflectivity across all bands, with a slight increase in the near-infrared bands. This slight increase occurs because near-infrared light penetrates beneath the ink layer and reflects off the underlying parchment (Figure 5).

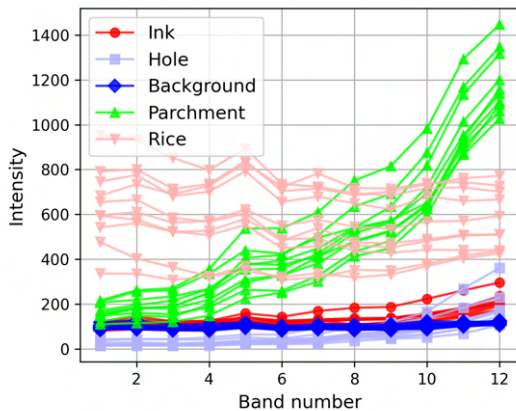


Fig. 5 The spectral behavior of ink, parchment, background, hole, and rice paper materials within a DSS fragment, measured across 12 spectral bands. Each curve represents the reflectance profile of a manually selected representative pixel from each material class. This analysis highlights which spectral bands are most discriminative for segmenting ink and parchment regions.

3.2.2 Normalization

The full-color images and normalized last-band images were included in the dataset for qualitative evaluation and potential future work. The full-color image reveals details without requiring additional processing. In contrast, the raw 16-bit last-band image, despite having the highest contrast between the ink and parchment, does not appear clearly to the eye because its pixel values are concentrated in a narrow range relative to the full span of 0–65535. Therefore, a normalized version of the last-band images was included to enhance visibility.

Since the raw images are stored as integer intensity values, gamma encoding was applied before normalization. Let $I(x, y)$ denote the pixel intensity at location (x, y) in the raw 16-bit last-band image. The image is first scaled to the unit range $[0, 1]$:

$$I_{\text{unit}}(x, y) = \frac{I(x, y)}{65535} \quad (1)$$

Next, gamma encoding is applied using the equation:

$$I_{\text{gamma}}(x, y) = I_{\text{unit}}(x, y)^{1/\gamma} \quad (2)$$

where $\gamma = 2.2$, which is a standard choice. After gamma encoding, the resulting image is

normalized to the range [0, 65535]:

$$I_{\text{normal}}(x, y) = 65535 \cdot \frac{I_{\text{gamma}}(x, y) - \min(I_{\text{gamma}})}{\max(I_{\text{gamma}}) - \min(I_{\text{gamma}})} \quad (3)$$

Finally, the image is converted back to a 8-bit format and saved as a JPEG file for ease of use.

3.3 Annotation

We performed manual pixel-level annotation using GIMP on the normalized infrared images, as they provided the clearest visualization of ink and parchment regions. A transparent annotation layer was placed over each image, and pixels were manually assigned to one of three classes: ink, parchment, or background. Ink pixels were marked with one color, parchment pixels with another, and all remaining pixels were designated as background. This resulted in a complementary labeling, where each pixel was assigned to exactly one of the three mutually exclusive classes. Separate binary masks were generated for each class and stored as ground truth.

3.4 Pixel-level class distributions

To better understand the distribution of content across the annotated QSD fragments, we computed the pixel-wise area occupied by each region class, **ink**, **parchment**, and **background**, in all 20 annotated images. These statistics are derived from the final masks used for evaluation.

Figure 6 shows a stacked bar chart displaying the proportion of each region type across individual images. On average, **background** occupies 71.1% of the image area, **parchment** 27.1%, and **ink** only 1.8%. These figures highlight the highly imbalanced nature of the task, especially the relatively small presence of ink pixels.

4 Method

We are ready to present the Multispectral Thresholding and Energy Minimization (MTEM) method for segmenting ink and parchment regions in high resolution images of Dead Sea Scroll (DSS) fragments. Given the challenges of manual annotation, due to the intricate features and physical deformations of the fragments, our approach combines multispectral thresholding with energy minimization to distinguish ink, parchment, and other

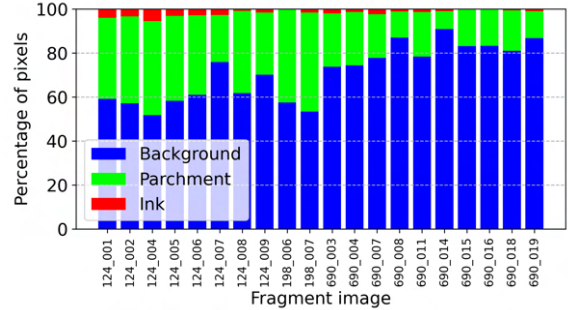


Fig. 6 Proportion of ink, parchment, and background regions across annotated QSD fragments.

regions such as background, holes, and rice paper. By analyzing spectral characteristics across multiple bands, we identify distinctive intensity trends that allow for thresholding. The initial segmentation is then refined using energy minimization, yielding delineation of ink and parchment from other regions.

4.1 Method motivation

Annotating DSS fragments is particularly challenging due to the high resolution of the images (7216×5412 pixels), which capture fine-grained and important details requiring expert interpretation. The physical characteristics of the fragments further complicate the annotation process. Parchment edges are often highly irregular and deformed, making accurate boundary delineation difficult. Ink regions are frequently faded or fragmented, increasing the complexity and length of the contours to be segmented. The task becomes even more difficult in darkened areas of the parchment, where distinguishing ink from the underlying material is visually ambiguous. Additionally, holes in the parchment closely resemble ink in both shape and tone, further complicating their differentiation. Although near-infrared imaging improves ink visibility on parchment, it is insufficient for clearly distinguishing ink from background, holes and darkened parchment (Figure 7).

4.2 Proposed solution

Given these challenges, we aimed to develop an ink and parchment segmentation method that eliminates the need for manual, expert-driven

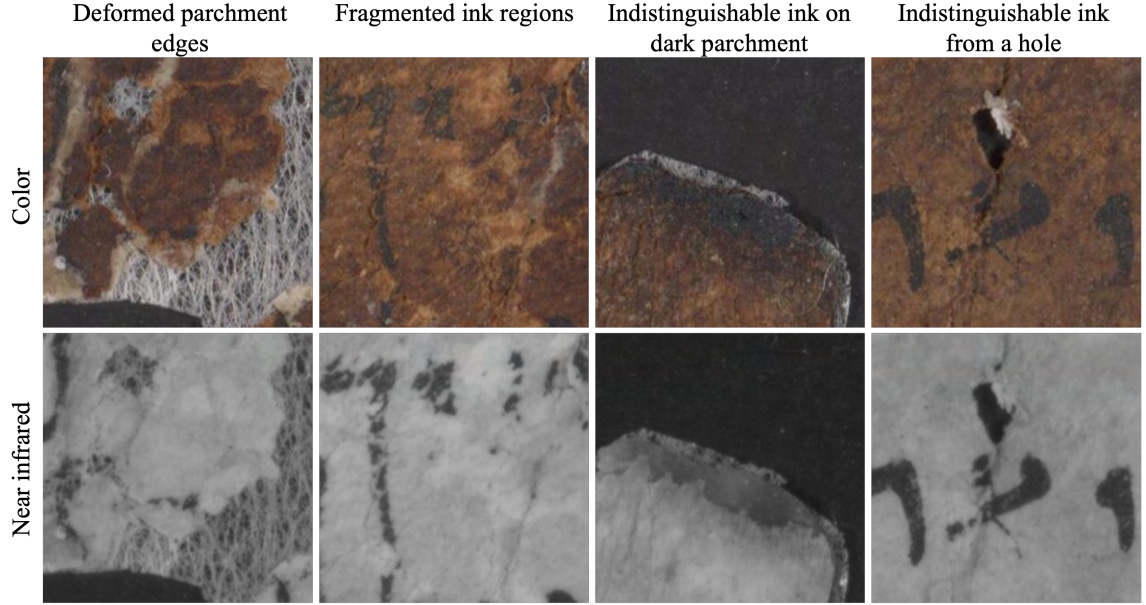


Fig. 7 DSS fragment image patches illustrating various annotation challenges. The first row shows color images highlighting deformed parchment edges, fragmented ink regions, indistinguishable ink on dark parchment, and ink that is difficult to differentiate from a hole. The second row displays corresponding near-infrared images, which, while enhancing ink visibility on normal parchment, fail to reveal clear ink edges on darkened parchment and do not help to differentiate ink from background and holes

annotation by providing an automated solution to support the analysis of DSS fragments.

Due to the high cost of manual labeling, our method is designed to operate without expert annotated data. We leverage the multispectral images provided by the IAA, where each DSS fragment is photographed in 12 wavelengths (7 visible and 5 near-infrared). We analyzed the spectral trends of different regions across the 12 bands (Figure 5) and observed that the 12th and 1st bands provide the highest contrast for differentiating ink, parchment, and other regions such as background, holes, and rice paper, the latter of which largely consists of background pixels due to its perforated structure.

4.2.1 Thresholding ink contours and parchment

Multispectral thresholding is sufficient to segment the parchment from all other regions. However, it is not effective for separating low-contrast regions such as ink, background, and holes, whose spectral trends overlap. Although ink and background exhibit similar intensity values, we leverage a key insight: the contour regions surrounding ink

strokes display higher reflectance due to the thin layer of ink partially absorbed into the parchment. We identify these contour pixels via thresholding and use them as seed regions for subsequent ink segmentation.

4.2.2 Energy minimization for segmenting ink from background

With the parchment and ink contours thresholded, we isolate the inverse parchment regions namely, ink, background, holes, and rice paper. We then apply energy minimization to segment the ink regions by pulling these inverse parchment regions toward the ink contours, while simultaneously pulling the background, holes, and rice paper toward the parchment. This process relies on the assumption that ink regions are spatially closer to ink contours than to parchment, whereas background, hole, and rice paper regions are more proximate to parchment than to the ink contours (Figure 14).

4.3 Multispectral characterization

Given a fragment image, our goal is to segment the ink and parchment regions. In other words, we aim

to identify the pixels corresponding to the ink and those corresponding to the parchment. However, a fragment image also contains additional regions beyond ink and parchment, such as background, holes, and rice paper. While we do not need to differentiate between the background, hole, and rice paper regions, it is crucial to distinguish them from the ink and parchment regions. To identify the most discriminative bands or band differences for segmentation of ink and parchment, we randomly sample pixels from each of the five region types ink, parchment, background, holes, and rice paper, and analyze their multispectral intensity trends.

Figure 5 illustrates the multispectral intensity trends for each region across the 12 spectral bands. We observe that parchment exhibits a highly distinctive trend from background, holes, and rice paper, marked by significantly higher reflectivity in the near-infrared bands. Rice paper also shows a unique trend that remains relatively consistent, with minimal overlap with the intensity values of ink. In contrast, the trends for ink, holes, and background are more similar and tend to overlap, displaying small variances. Background pixels maintain a consistent intensity across all bands but have similar values to those of ink. Hole intensities are closely grouped in the initial bands but increase in the final bands, where they start to overlap with ink, which also shows an increase in intensity. The reflectivity increase in ink regions is attributed to near-infrared light penetrating the ink layer and scattering off the underlying parchment. The reflectivity increase in hole regions is due to diffusive reflection of near-infrared light from the surrounding parchment edges near the hole.

We hypothesize that the diffusive reflectivity also contributes to halos in the IAA images, which become particularly prominent in the near-infrared bands (Figure 8). This is due to the higher reflectivity of parchment in those bands, making the halos visible in background areas adjacent to parchment regions. This observation also supports the reasoning regarding the holes, explaining why they appear to have slightly higher reflectivity than the background: they are surrounded by parchment and affected by strong diffusive reflections. Thus, for holes to be classified as such, they should remain relatively small; beyond a

certain size, they start behaving more like the background.

Figure 5 reveals that parchment pixels achieve the best discrimination using the intensity difference between band 12 and band 1, denoted as $I_{12} - I_1$, where I_n represents the image of band n . This band difference emphasizes the uniquely increasing trend of parchment in contrast to all other regions, as shown in Figure 9. Similarly, ink pixels are best distinguished when using a combination of $I_{12} - I_1$ and I_1 , where I_1 helps to exclude hole and rice paper pixels, while the $I_{12} - I_1$ difference helps to exclude parchment and background pixels (Figure 10).

4.4 Multispectral thresholding

After identifying that parchment can be distinguished using the intensity difference $I_{12} - I_1$ and ink can be distinguished using a combination of $I_{12} - I_1$ and I_1 , we employed annotations from the fragment 124-001 to set thresholds for differentiating parchment and ink from other regions. For each of the ink and parchment regions, we applied a percentile based method using region specific intensity values from the annotated fragment. Percentiles allow us to set thresholds by focusing on the central distribution of pixel intensities, reducing the influence of extreme values or noise. The n -th percentile, denoted as P_n , is the value below which $n\%$ of the data falls. Accordingly, we defined the lower threshold for each region as its P_n value and the upper threshold as its P_{100-n} value, thus capturing the primary intensity range while excluding outliers.

4.4.1 Finding the threshold values for extracting parchment and ink

For thresholding parchment, we applied the n -th percentile on $I_{12} - I_1$ because multispectral characterization indicated that $I_{12} - I_1$ provides a discrimination between parchment and other regions.

For thresholding ink, we applied the n -th percentile on both I_1 and $I_{12} - I_1$, as multispectral characterization demonstrated that the combination of I_1 and $I_{12} - I_1$ can distinguish ink from other regions.

Figure 11 illustrates that, as the percentile threshold decreases, segmentation for both ink and parchment becomes more complete but also

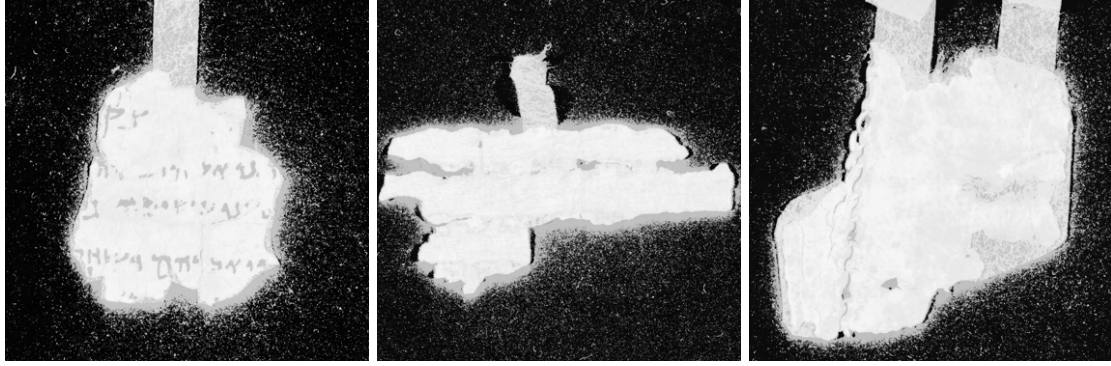


Fig. 8 Equalized last-band images of three DSS fragments showing halos at the edges of the parchment. We hypothesize that the halos and holes are background regions influenced by diffusive reflections from the parchment in near-infrared bands, where the higher reflectivity of parchment makes these effects prominent

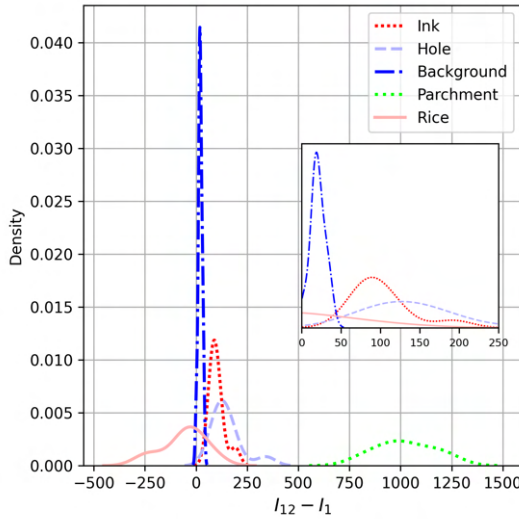


Fig. 9 Intensity distribution of $I_{12} - I_1$ across different regions, illustrating the separability of parchment pixels from other regions

incorporates more noise from other regions; conversely, as the percentile increases, segmentation becomes less complete but contains less noise. Based on the experimental assessment in Section 5.4, we chose $n = 10$ for parchment thresholding that includes the maximum parchment pixels with the least noise pixels. However, the segmented parchment alone is not the primary focus; scholars are more interested in the combined parchment+ink regions, which requires accurate ink segmentation for effective parchment segmentation.

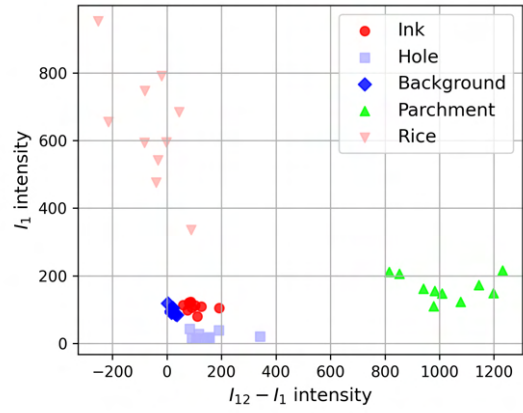


Fig. 10 Combination of I_1 and $I_{12} - I_1$ values across different regions, illustrating the separability of ink pixels from other regions

Notably, none of the tested n values yield satisfactory ink segmentation. Ink regions encompass not only ink but also cracks, fading, holes, and degraded parchment. We chose $n = 10$ for ink thresholding, based on the assessment of Section 5.4, which includes the maximum ink pixels with the fewest noise pixels.

An interesting observation is that ink contours may serve as the most reliable areas, preserving the shape information of the ink while minimizing internal ink region noise interference. Furthermore, the multispectral trend of ink contours differs significantly from that of holes and background due to their thinner ink layer, which allows greater influence from the underlying parchment. This makes ink contours more distinguishable than ink pixels alone (Figure 12).

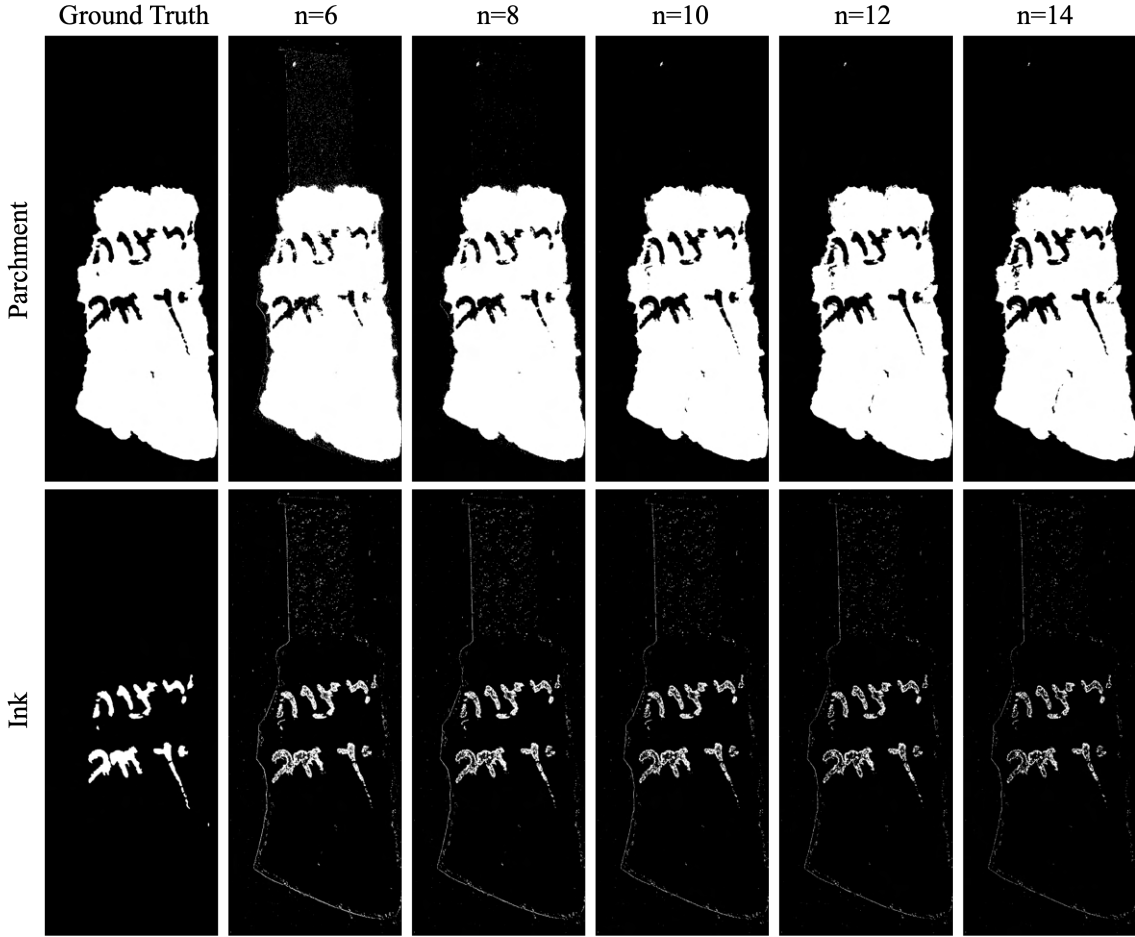


Fig. 11 Multispectral thresholding results of parchment and ink regions with varying percentiles with the first column as ground truth

4.4.2 Finding threshold values for extracting ink contours

To determine appropriate threshold values for extracting ink contours, we used fragment 124_001. Ink contours were derived from the ground truth ink mask by outlining the boundaries of the ink regions and rendering them with a contour thicknesses of t pixel. The experiments of Section 5.4 suggest choosing $t = 1$ for ink contour thresholding. Within the resulting ink contour mask, we extracted pixel intensities from both I_1 and the difference image $I_{12} - I_1$. For each, we computed the 10th and 90th percentiles of the intensity distribution. These percentile values served as lower and upper bounds for defining the intensity range of ink contours. Using these thresholds, we constructed a binary mask for

ink contours which effectively highlighted the ink contours (Figure 13).

4.5 Energy Minimization

In this section, we formulate an energy minimization approach to enhance the segmentation of ink and parchment regions in binary document images. We begin by defining an energy function for the segmentation task, balancing the cost of assigning pixels to certain labels with the desire for smoothness between neighboring pixels. We then show how this general energy minimization framework is specifically adapted to our problem. By incorporating initial masks obtained from multispectral thresholding, we tailor the energy function to refine the ink contour masks and

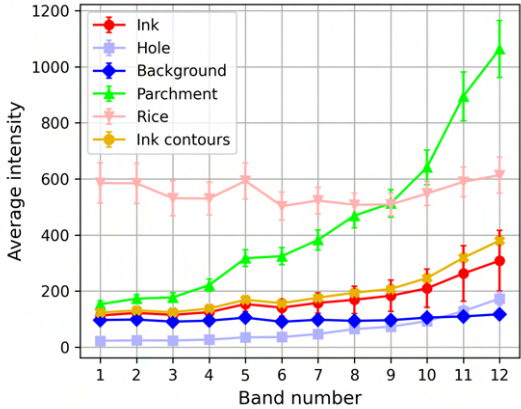


Fig. 12 Average intensity trends showing that ink contours are more distinguishable than ink regions due to their thinner ink layer, allowing greater influence from the underlying parchment

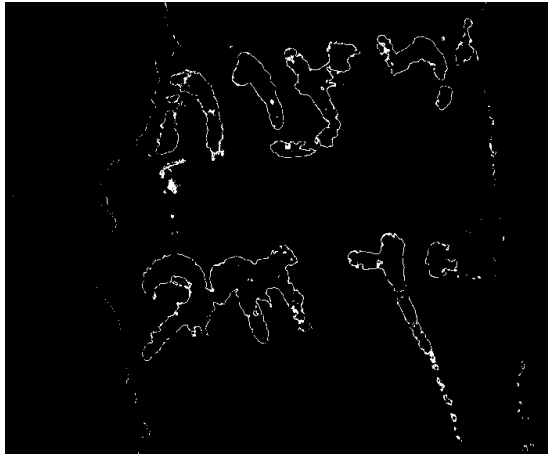


Fig. 13 Multispectral thresholding result for ink contours using a percentile of $n = 10$

improve the delineation between ink, parchment, and other regions.

4.5.1 Energy minimization formulation

Let $\mathcal{L} = \{\ell_0, \ell_1\}$ be the set of binary labels corresponding to two distinct spatial classes, and let \mathcal{P} be the set of candidate pixels to be segmented, specifically defined as the white pixels in a binary input mask. Energy minimization seeks a labeling function f that assigns each pixel $p \in \mathcal{P}$ a label $\ell_p \in \mathcal{L}$, such that the total energy $\mathbf{E}(f)$ is minimized:

$$\mathbf{E}(f) = \sum_{p \in \mathcal{P}} D(p, \ell_p) + \sum_{\{p, p'\} \in \mathcal{N}} d(p, p') \cdot \delta(\ell_p \neq \ell_{p'}) \quad (4)$$

Here, $D(p, \ell_p)$ is the data cost of assigning label ℓ_p to pixel p , and $d(p, p')$ is the smoothness cost that penalizes label discontinuities between neighboring pixels. $\delta(\ell_p \neq \ell_{p'})$ is an indicator function that equals 1 if the labels differ and 0 otherwise.

The smoothness cost encourages spatial coherence by penalizing label differences between neighboring candidate pixels. Let \mathcal{N} denote the set of 4-connected neighboring pixel pairs in \mathcal{P} . The smoothness cost $d(p, p')$ is defined as:

$$d(p, p') = \begin{cases} 1, & \text{if } \{p, p'\} \in \mathcal{N} \\ 0, & \text{otherwise} \end{cases} \quad (5)$$

We minimize the energy function using a graph-cut based max-flow/min-cut algorithm, which efficiently assigns binary labels to pixels while encouraging spatial consistency between neighboring pixels [62].

4.5.2 EM Adaptation for segmenting ink and parchment

As illustrated in Figure 14, which shows the inputs and outputs at different stages of our method pipeline, we begin with three binary masks derived from multispectral thresholding (Section 4.4): a parchment mask M_P , an ink mask M_I , and an ink contour mask M_C .

To obtain a mask for all other regions, denoted M_O , we calculate the complement of the union of M_P , M_I , and M_C :

$$M_O = (M_P \cup M_I \cup M_C)' \quad (6)$$

Ink contours tend to be more distinguishable from the background and holes, but the mask M_C is often noisy. It includes stray pixels from non-ink regions and is discontinuous when ink regions are located at the edge of background or hole regions. To refine this mask, we apply energy minimization to classify pixels in M_C as either belonging to parchment-adjacent boundaries or to noise. This refinement is based on the assumption that clean ink contours are spatially closer to

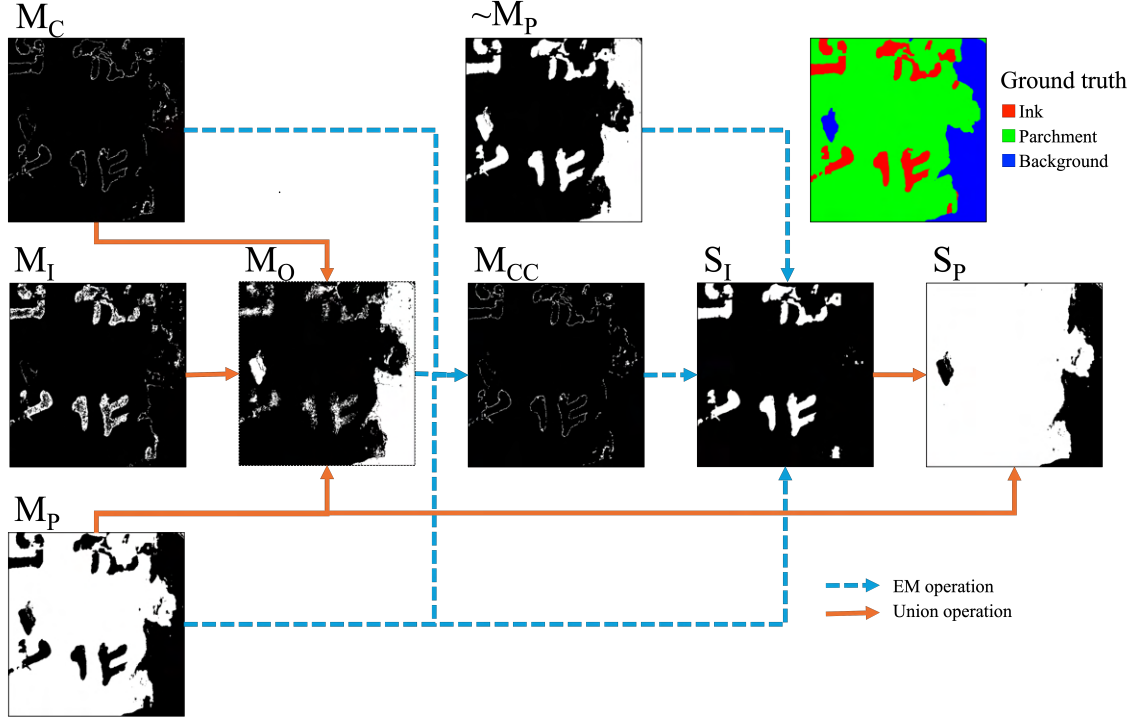


Fig. 14 Image patches representing the inputs and outputs at different stages of the whole method pipeline. Red arrows indicate the union operation, while blue arrows denote the EM operation. The final outputs of the method are the ink segmentation (S_I) and parchment segmentation (S_P). The ground truth (GT) shows ink in red, parchment in green, and background in blue.

parchment, while noisy ink contours tend to be closer to background, hole, and rice paper regions.

We define a binary labeling function $f : M_C \rightarrow \{0, 1\}$, where:

- label 0 denotes non-parchment regions (e.g., background, holes, and rice paper), using M_O as a spatial prior;
- label 1 denotes parchment-adjacent regions, using M_P as a spatial prior.

The data term $D(p, \ell)$ is computed using Euclidean distance transforms. For each pixel $p \in M_C$, we calculate its distance to the nearest pixel in the prior mask corresponding to label ℓ (either M_O or M_P), and convert this distance into an inverse-distance-based cost.

Minimizing the energy function assigns each pixel in M_C to the label with the lower spatial cost while encouraging spatial coherence. The refined ink contour mask, denoted M_{CC} , is defined as the set of pixels labeled as parchment-adjacent:

$$M_{CC} = \{p \in M_C \mid f(p) = 1\} \quad (7)$$

Next, we apply a second round of energy minimization to extract the ink segmentation, denoted S_I . Let the binary labeling function $f : M'_P \rightarrow \{0, 1\}$ be as follows:

- label 0 corresponds to non-ink regions using M_P as a spatial prior;
- label 1 corresponds to ink regions using M_{CC} as a spatial prior.

Again, the data term is computed by inverse-distance transforms relative to the corresponding spatial prior mask. This labeling draws the non-parchment region toward either ink or non-ink classes based on spatial proximity. The result is a clean segmentation of the ink:

$$S_I = \{p \in M'_P \mid f(p) = 1\} \quad (8)$$

Finally, we define the parchment segmentation S_P as the union of the initial parchment mask and the inferred ink segmentation:

$$S_P = M_P \cup S_I \quad (9)$$

5 Experiments

We conducted a series of experiments aimed at answering key questions and determining optimal parameter values for the MTEM method. For the evaluation of segmentation results, we used the metrics, Intersection over Union (IoU), F_1 -score, precision, and recall.

5.1 Time efficiency

We evaluated the time efficiency of the MTEM method by measuring execution time for each image in relation to its size. The experiments were conducted using a single Intel Xeon CPU and 12 GB of RAM. Figure 15 demonstrates that processing time increases with image size. We observed that larger images of approximately 20 million pixels, required over 300 seconds to process, while smaller images of approximately 500,000 pixels had processing times of only around 5 seconds. This suggests a roughly linear relationship between image size and processing time. The average processing time for an image from the QSD is 54 seconds. The Pearson correlation coefficient between image size and processing time is 0.91, with a p -value of 2.1×10^{-8} , confirming a significant linear relationship. These results highlight the scalability of the method, but also indicate the possible need for optimization with larger image sizes.

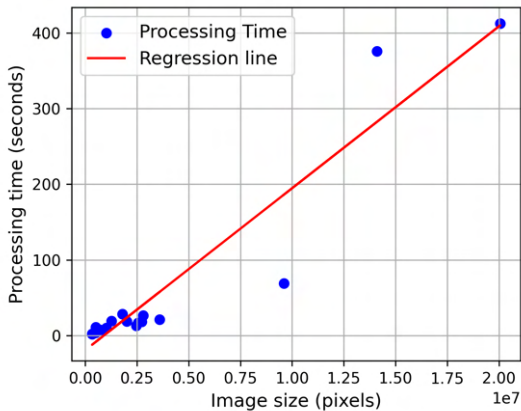


Fig. 15 Relationship between image size and processing time for the MTEM segmentation method. The plot illustrates that processing time increases approximately linearly with the size of the input image

5.2 Effectiveness of cleaning ink contours from noise

We conducted experiments to assess the impact of cleaning the ink contours from noise by comparing two different segmentation results: one using noisy ink contours (M_C) and another using cleaned ink contours (M_{CC}). Ink contours exhibit a distinct multispectral trend compared to both ink regions and parchment regions. The trend of ink contour regions falls between that of ink and parchment, allowing them to serve as useful features for segmentation. However, noisy pixels with similar intensity values may be present in other regions, introducing errors. It is assumed that clean ink contours are positioned close to parchment regions, given that ink is present on the surface parchment. Therefore, we utilized M_O to shrink the influence of the noise regions, and M_P to expand the influence of the clean ink contours. Table 2 presents the metrics obtained from both experiments.

The results indicate that using cleaned ink contours improves ink segmentation (S_I) performance. The high recall and low precision values with noisy contours indicates that S_I included more pixels from the other regions and M_P remain unaffected but the final parchment segmentation, $S_P = M_P \cup S_I$, is influenced by the errors introduced from S_I (Figure 16).

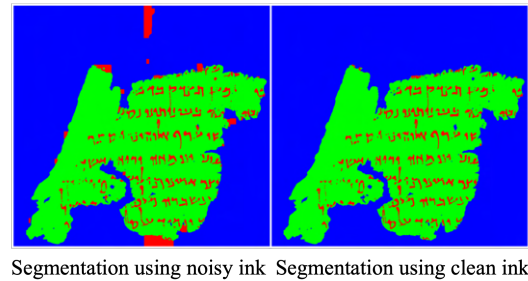


Fig. 16 Comparison of segmentation results with noisy vs. cleaned ink contours

5.3 Effectiveness of ink contour thickness

Having established that ink contours are critical for the performance of the MTEM method, an important question arises: what is the optimal

Table 2 Comparison of segmentation results with noisy vs. cleaned ink contours

Method	IoU	Precision	Recall	F ₁ -score
Ink (Noisy Contours)	0.199	0.224	0.695	0.260
Ink (Clean Contours)	0.671	0.894	0.703	0.768
Parchment (Noisy Contours)	0.636	0.640	0.991	0.742
Parchment (Clean Contours)	0.976	0.995	0.982	0.988

thickness of these contours to maximize segmentation quality? To address this, we extracted ink contours with varying thickness values t from the annotations of fragment 124_001. These were used to compute the $n = 10$ percentile thresholds for both I_1 and $I_{12} - I_1$, denoted respectively as I_1 lower, I_1 higher and $I_{12} - I_1$ lower, $I_{12} - I_1$ higher.

We then evaluated how different contour thickness values influenced the segmentation performance for ink and parchment regions. The results show that contour thickness plays a significant role in differentiating ink from other regions such as background, holes, and rice paper. As the contour thickness increases, the segmentation performance for ink (S_I) initially decreases and then stabilizes, while the performance for parchment (S_P) remains stable (Figure 17).

This trend can be explained by the fact that parchment segmentation is performed using fixed thresholding and is independent of ink contour detection, hence its stability. In contrast, ink segmentation relies on the contour to attract nearby ink pixels. As contour thickness increases, more pixels are included from both the ink region and the surrounding parchment. The additional pixels—mostly from within the parchment do not degrade performance significantly unless they approach confusing regions such as background, holes, or rice paper.

Additionally, we observe that increasing contour thickness leads to a rise in $I_{12} - I_1$ higher and a drop in $I_{12} - I_1$ lower, indicating that thicker contours progressively include more pixels from both ink and parchment regions (Figure 18). In contrast, the thresholds I_1 lower and I_1 higher for I_1 remain relatively constant across all thickness levels, suggesting that I_1 alone is insufficient for distinguishing ink contours from parchment. This observation is further supported by the two-dimensional distribution shown in Figure 10.

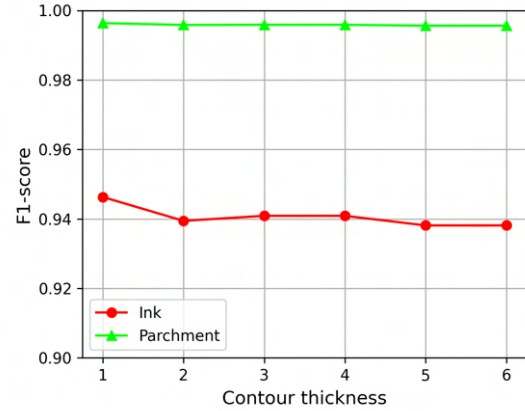


Fig. 17 Effect of contour thickness on performance

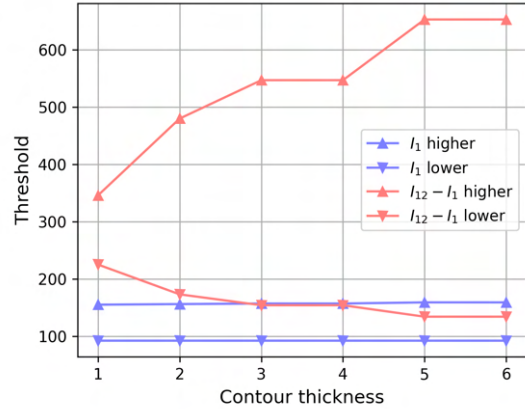


Fig. 18 Effect of contour thickness on threshold values

5.4 Optimal percentile

We explore the optimal percentile for the performance of the MTEM method in ink and parchment segmentation. The results (Figure 19) for ink segmentation indicate that the choice of percentile has a significant impact on performance. At all tested values of n , the ink segmentation F₁-score was almost zero, except when $n = 10$. For parchment segmentation, $n = 10$ also proved to be the optimal value, although its trend across

all n values remained relatively consistent. This is because the separability bounds for ink are very close to those of other regions, while the separability bounds for parchment are much more distinct from the other regions, as illustrated in Figure 10.

Overall, the results suggest that the optimal percentile value is $n = 10$ and highlight the need for careful selection of percentile thresholds to ensure robust performance. That said, since the percentile threshold is applied in a rule-based rather than learned fashion, we expect a reasonable tolerance range around the optimal value. Small deviations (e.g., $n = 9$ or $n = 11$) are unlikely to substantially affect segmentation quality.

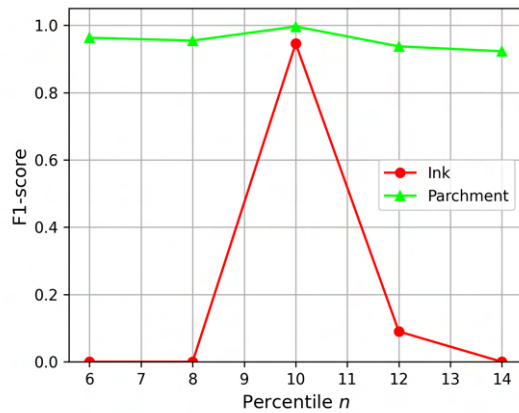


Fig. 19 Effect of percentile value n on the segmentation performance for ink and parchment. The figure illustrates that $n = 10$ yields the highest F_1 -score, especially for ink segmentation

6 Results

6.1 Quantitative Results

In this section, we present the evaluation of various ink and parchment segmentation methods applied to QSD images. The evaluated methods include the proposed MTEM method for both ink and parchment segmentation, along with traditional binarization techniques such as Otsu and Sauvola for parchment segmentation. For a fair comparison, Otsu and Sauvola thresholding were applied to the normalized infrared images corresponding to the last spectral band, which offers

the highest contrast between the fragment and the background.

We emphasize that Otsu and Sauvola are applicable only to parchment segmentation and are not capable of distinguishing between ink and background. To the best of our knowledge, there is currently no unsupervised method in the literature that can segment dark ink from dark background in Dead Sea Scroll fragment images. As such, no direct comparison is possible for the ink segmentation task.

The evaluation metrics used to assess segmentation performance are Intersection over Union (IoU), precision, recall, and F_1 -score. The results are summarized in Table 3.

The proposed MTEM method for ink segmentation yields promising results, with an IoU of 0.6713. The precision is 0.8935, indicating that most of the detected ink pixels are indeed correct. However, the recall is 0.7029, suggesting that there is still room for improvement in capturing all ink pixels, as some are missed during detection. We observe that these missed pixels often occur in ink regions contaminated by unspecified substances (such as salt) or in ink areas on dark parchment surfaces, making their contours less detectable.

For parchment segmentation, the MTEM method performs exceptionally well, achieving an IoU of 0.9764. The high F_1 -score of 0.9877 further demonstrates the reliability of MTEM for parchment segmentation.

In contrast, the performance of the Otsu method, the Sauvola method, and their combination (via an AND operation) for parchment segmentation is notably lower compared to MTEM. The relatively low precision and high recall indicate that these methods tend to over-segment, capturing almost all potential parchment regions but also producing a significant number of false positives, especially in rice paper regions that have high reflectivity in the infrared images.

Overall, the results indicate that the MTEM method outperforms traditional binarization techniques such as Otsu and Sauvola for parchment segmentation. Specifically, MTEM demonstrates significantly higher IoU and F_1 -score, highlighting its effectiveness in detecting parchment areas. Additionally, the MTEM method segments ink regions and can distinguish ink areas from holes and background regions.

Table 3 Performance of different methods applied to QSD images for segmenting ink and parchment regions (excluding fragment 124_001, which was used for tuning)

Method	IoU	Precision	Recall	F ₁ -score
MTEM ink	0.658	0.889	0.690	0.757
MTEM parchment	0.976	0.994	0.981	0.987
Otsu parchment	0.551	0.573	0.948	0.681
Sauvola parchment	0.306	0.315	0.932	0.457
Otsu + Sauvola parchment	0.546	0.576	0.930	0.678

6.2 Qualitative results

To illustrate the effectiveness of the MTEM segmentation method, we present some QSD images and their segmented outputs using MTEM in Figure 20. Most importantly, MTEM can discriminate ink from holes and background, remove rice paper regions even when they are between the parchment and ink regions, and accurately delineate the edges of ink regions that are adjacent to the background or rice paper regions.

The majority of error cases occur when ink is present on a very dark parchment region. In such instances, the MTEM method apparently fails to extract the ink contours and consequently fails to segment the ink. A second type of error case we observed occurs on ink regions influenced by an unknown but apparently white substance, which prevents the ink contours from being extracted and, as a result, the ink region cannot be segmented.

7 Conclusion

The proposed Multispectral Thresholding and Energy Minimization (MTEM) method addresses the challenges of segmenting parchment and separating dark ink from the dark background. Unlike traditional binarization methods, MTEM segments not only parchment and background, but also ink regions that is visually similar to the dark background. This is achieved by leveraging the physical blending effect that occurs at ink-parchment boundaries, where ink absorption into the parchment produces high-reflectivity contour regions. MTEM thresholds and uses these ink contours to pull adjacent pixels into the ink region, effectively distinguishing dark ink from dark background, which lacks such blending characteristics.

The proposed method has the potential for application to other multispectral image datasets,

such as the MultiSpectral Document Binarization (MSBIN) dataset [63], the MultiSpectral Text Extraction (MS-TEx) dataset [64], and the Multispectral Hebrew Ostraca dataset [46].

Future work will extend these segmentation to improve kraken’s [65] character identification and correct inaccurate detections, enabling precise character segmentation. By integrating segmented characters and parchments, further analyses of DSS images will be facilitated, including the alignment of transcriptions with images to add a searchable textual layer to the IAA images, allowing scholars to locate text in its spatial context.

References

- [1] Zuckerman, B.: The dynamics of change in the computer imaging of the Dead Sea scrolls and other ancient inscriptions. Rediscovering the Dead Sea Scrolls: An Assessment of Old and New Approaches and Methods, 69–88 (2010)
- [2] Avigad, N., Yadin, Y.: A Genesis Apocryphon: A Scroll from the Wilderness of Judaea. Magnes Press of the Hebrew University, Jerusalem, Israel (1956)
- [3] Oprescu, A., Rosengarten, O., Shor, P.: Multispectral imaging and the digitization of the Dead Sea Scrolls. Book and Paper Group Annual **37**, 71–76 (2018)
- [4] Israel Antiquities Authority: The Leon Levy Dead Sea Scrolls Digital Library. Accessed: 16 March 2025 (2025). https://www.deadseascrolls.org.il/?locale=en_US
- [5] Driscoll, M.J., Pierazzo, E.: Digital Scholarly Editing: Theories and Practices. Open Book Publishers, Cambridge, UK (2016)

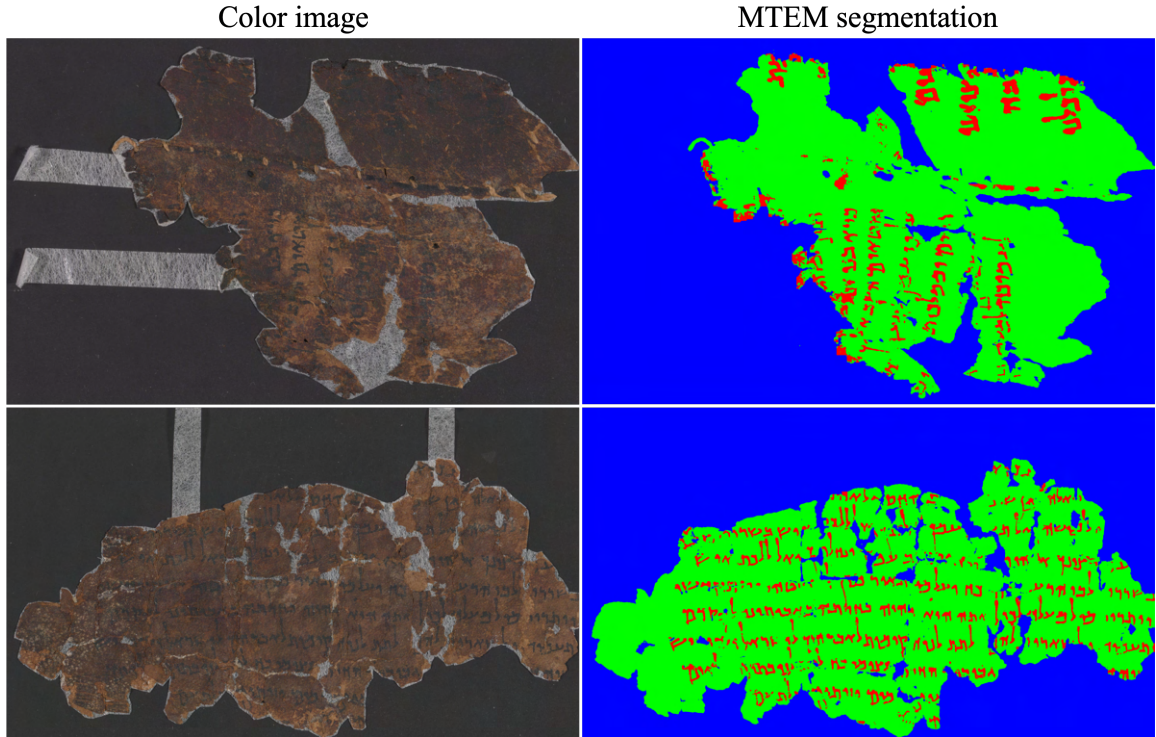


Fig. 20 Qualitative results demonstrating the effectiveness of the MTEM segmentation method. The left column shows the QSD color images, while the right column displays their segmentation using MTEM. In the segmentation images, ink is represented in red, parchment in green, and background in blue. The MTEM method can discriminate ink from holes and background, removes rice paper regions even when they are between the parchment and ink regions, and accurately delineates the edges of ink regions that are adjacent to the background or rice paper regions

- [6] Robinson, P.: What is a critical digital edition? Variants: The Journal of the European Society for Textual Scholarship **1**, 43–62 (2002)
- [7] Garcia Martinez, F., Tigchelaar, E.J.: The Dead Sea Scrolls Study Edition. Brill, Leiden (2000)
- [8] Machiela, D.: The Dead Sea Genesis Apocryphon: A New Text and Translation with Introduction and Special Treatment of Columns 13–17. Brill, Leiden (2009)
- [9] Ulrich, E.: The Biblical Qumran Scrolls: Transcriptions and Textual Variants. Brill, Leiden (2010)
- [10] Ulrich, E.: Identification of a scribe active at Qumran: 1QPsib-4QIsac-11QM. Meghillot: Studies in the Dead Sea Scrolls **6**, 201–210 (2007)
- [11] Brown-deVost, B.: Scripta Qumranica Electronica (2016–2021). Hebrew Bible and Ancient Israel **5**(3), 307–315 (2016)
- [12] Gayer, A.: A new reconstruction of the “Wisdom of the Hands” unit in 4QInstructiond (4Q418). Journal for the Study of the Pseudepigrapha **30**(2), 60–73 (2020)
- [13] Tucker, J.M.: From ink traces to ideology: Material, text, and composition of Qumran community rule manuscripts. PhD thesis, University of Toronto (2021)
- [14] Ben-Dov, J., Gayer, A., Ratzon, E.: Material and Digital Reconstruction of Fragmentary Dead Sea Scrolls: The Case of 4Q418a. Brill, Leiden (2022)
- [15] Hayes, G.: Searching for Dead Sea scribes. PhD thesis, University of Groningen (2023)

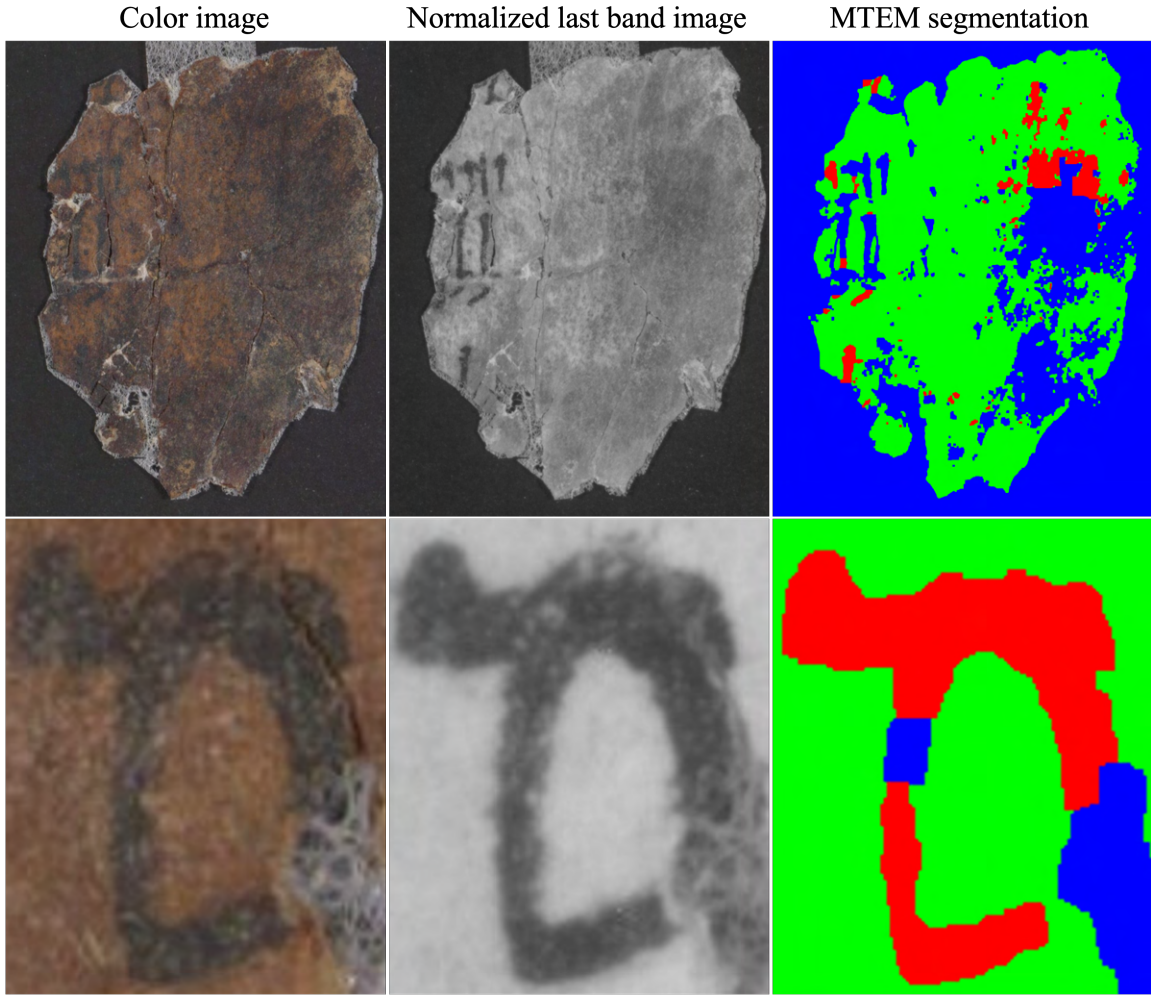


Fig. 21 Illustration of error cases in MTEM segmentation. The left column shows the QSD color images, the middle column displays the normalized last band images, and the right column presents the MTEM segmentation results. In the first example, ink is present on a very dark parchment region, causing the MTEM method to fail in extracting the ink contours and consequently fail to segment the ink. In the second example, the ink regions are influenced by an unknown but apparently white substance, which prevents the ink contours from being extracted, and as a result, the ink regions cannot be segmented

- [16] Ben-Dov, J., Gayer, A., Ratzon, E.: A protocol for material and digital reconstruction of fragmentary dead sea scrolls. In: Sion, O., Uziel, J., Ganor, A., Klein, E. (eds.) New Studies in the Archaeology of the Judean Desert: Collected Papers, pp. 333–355. Israel Antiquities Authority, Jerusalem, Israel (2023)
- [17] Stökl Ben Ezra, D., Brown-DeVost, B., Dershowitz, N., Pechorin, A., Kiessling, B.: Transcription alignment for highly fragmentary historical manuscripts: The Dead Sea Scrolls. In: 17th International Conference on Frontiers in Handwriting Recognition (ICFHR), pp. 361–366 (2020). IEEE
- [18] Dhali, M., He, S., Popović, M., Tigchelaar, E., Schomaker, L.: A digital palaeographic approach towards writer identification in the Dead Sea Scrolls. In: International Conference on Pattern Recognition Applications and Methods 2017, pp. 693–702 (2017)
- [19] Dhali, M.A., Jansen, C.N., De Wit, J.W., Schomaker, L.: Feature-extraction methods

- for historical manuscript dating based on writing style development. *Pattern Recognition Letters* **131**, 413–420 (2020)
- [20] Popović, M., Dhali, M.A., Schomaker, L.: Artificial intelligence based writer identification generates new evidence for the unknown scribes of the Dead Sea Scrolls exemplified by the Great Isaiah Scroll (1QIsaa). *PLOS ONE* **16**(4), 0249769 (2021)
- [21] Koopmans, L., Dhali, M.A., Schomaker, L.: The Effects of Character-Level Data Augmentation on Style-Based Dating of Historical Manuscripts. In: Proceedings of the 12th International Conference on Pattern Recognition Applications and Methods – Volume 1: ICPRAM, pp. 124–135. SciTePress, Setúbal, Portugal (2023)
- [22] Koopmans, L., Dhali, M.A., Schomaker, L.: Performance analysis of handwritten text augmentation on style-based dating of historical documents. *SN Computer Science* **5**(4), 397 (2024)
- [23] Reynolds, T., Dhali, M., Schomaker, L.: Image-based material analysis of ancient historical documents. In: 12th International Conference on Pattern Recognition Applications and Methods (ICPRAM), Setúbal, Portugal, pp. 697–706 (2023). SciTePress
- [24] Dhali, M.A., Reynolds, T., Alizadeh, A.Z., Nijdam, S.H., Schomaker, L.: Pattern recognition techniques in image-based material classification of ancient manuscripts. In: International Conference on Pattern Recognition Applications and Methods, pp. 124–150 (2023). Springer
- [25] Ratzon, E., Dershovitz, N.: The length of a scroll: Quantitative evaluation of material reconstructions. *PLoS ONE* **15**(10), 0239831 (2020)
- [26] Brown-Devost, B., Dershovitz, N., Stökl Ben Ezra, D.: Automatically linking Dead Sea Scroll transcriptions to fragment images: Towards the letter level. In: Proceedings of the 11th Congress of the International Organization for Qumran Studies (IOQS) (2022)
- [27] Levi, G., Nisnevich, P., Ben-Shalom, A., Dershovitz, N., Wolf, L.: A method for segmentation, matching and alignment of Dead Sea Scrolls. In: IEEE Winter Conference on Applications of Computer Vision (WACV), pp. 208–217 (2018). IEEE
- [28] Badamdjorj, T., Ben-Shalom, A., Dershovitz, N.: Matching and searching the Dead Sea Scrolls. In: IEEE International Conference on the Science of Electrical Engineering in Israel (ICSEE), pp. 1–5 (2018). IEEE
- [29] Uzan, L., Dershovitz, N., Wolf, L.: Qumran letter restoration by rotation and reflection modified PixelCNN. In: 14th IAPR International Conference on Document Analysis and Recognition (ICDAR), vol. 1, pp. 23–29 (2017). IEEE
- [30] Dhali, M.A., Wit, J.W., Schomaker, L.: BiNet: Degraded-manuscript binarization in diverse document textures and layouts using deep encoder-decoder networks. arXiv preprint arXiv:1911.07930 (2019)
- [31] Lavee, T.: Computer analysis of the Dead Sea Scroll manuscripts. Master’s thesis, School of Computer Science, Tel Aviv University (September 2013)
- [32] Maor, Y., Shor, P., Aizenshtat, Z.: Parchment browning and the Dead Sea Scrolls – part I: Artificial aging. *Polymer Degradation and Stability* **176**, 109109 (2020)
- [33] Otsu, N.: A threshold selection method from gray-level histograms. *IEEE Transactions on Systems, Man, and Cybernetics* **9**(1), 62–66 (1979)
- [34] Niblack, W.: An Introduction to Digital Image Processing. Strandberg Publishing Company, Topstykket, Denmark (1985)
- [35] Sauvola, J., Seppanen, T., Haapakoski, S., Pietikainen, M.: Adaptive document binarization. In: Proceedings of the Fourth International Conference on Document Analysis and Recognition, vol. 1, pp. 147–152 (1997). IEEE

- [36] Lu, S., Su, B., Tan, C.L.: Document image binarization using background estimation and stroke edges. *International Journal on Document Analysis and Recognition (IJDAR)* **13**, 303–314 (2010)
- [37] Su, B., Lu, S., Tan, C.L.: Robust document image binarization technique for degraded document images. *IEEE Transactions on Image Processing* **22**(4), 1408–1417 (2012)
- [38] Wolf, C., Doermann, D.: Binarization of low quality text using a Markov random field model. In: *International Conference on Pattern Recognition*, vol. 3, pp. 160–163 (2002). IEEE
- [39] Gatos, B., Pratikakis, I., Perantonis, S.J.: Adaptive degraded document image binarization. *Pattern Recognition* **39**(3), 317–327 (2006)
- [40] Vo, Q.N., Kim, S.H., Yang, H.J., Lee, G.: Binarization of degraded document images based on hierarchical deep supervised network. *Pattern Recognition* **74**, 568–586 (2018)
- [41] Zhao, J., Shi, C., Jia, F., Wang, Y., Xiao, B.: Document image binarization with cascaded generators of conditional generative adversarial networks. *Pattern Recognition* **96**, 106968 (2019)
- [42] He, S., Schomaker, L.: DeepOtsu: Document enhancement and binarization using iterative deep learning. *Pattern Recognition* **91**, 379–390 (2019)
- [43] Kang, S., Iwana, B.K., Uchida, S.: Complex image processing with less data—Document image binarization by integrating multiple pre-trained U-Net modules. *Pattern Recognition* **109**(art. 107577), 1–13 (2021)
- [44] He, S., Schomaker, L.: CT-Net: Cascade T-shape deep fusion networks for document binarization. *Pattern Recognition* **118**, 108010 (2021)
- [45] Lettner, M., Kleber, F., Sablatnig, R., Miklas, H.: Contrast enhancement in multispectral images by emphasizing text regions. In: *The Eighth IAPR International Workshop on Document Analysis Systems*, pp. 225–232 (2008). IEEE
- [46] Faigenbaum, S., Sober, B., Shaus, A., Moinester, M., Piasetzky, E., Bearman, G., Cordonsky, M., Finkelstein, I.: Multispectral images of ostraca: Acquisition and analysis. *Journal of Archaeological Science* **39**(12), 3581–3590 (2012)
- [47] Salerno, E., Tonazzini, A., Bedini, L.: Digital image analysis to enhance underwritten text in the Archimedes palimpsest. *International Journal on Document Analysis and Recognition (IJDAR)* **9**(2), 79–87 (2007)
- [48] Easton, R.L., Knox, K.T., Christensen-Barry, W.A.: Multispectral imaging of the Archimedes palimpsest. In: *32nd Applied Imagery Pattern Recognition Workshop*, 2003. Proceedings., pp. 111–116 (2003). IEEE
- [49] Rapantzikos, K., Balas, C.: Hyperspectral imaging: Potential in non-destructive analysis of palimpsests. In: *IEEE International Conference on Image Processing*, vol. II, pp. 618–621 (2005). IEEE
- [50] Starynska, A., Messinger, D., Kong, Y.: Revealing a history: Palimpsest text separation with generative networks. *International Journal on Document Analysis and Recognition (IJDAR)* **24**(3), 181–195 (2021)
- [51] Lettner, M., Sablatnig, R.: Spatial and spectral based segmentation of text in multispectral images of ancient documents. In: *10th International Conference on Document Analysis and Recognition*, pp. 813–817 (2009). IEEE
- [52] Lettner, M., Sablatnig, R.: Multispectral imaging for analyzing ancient manuscripts. In: *17th European Signal Processing Conference*, pp. 1200–1204 (2009). IEEE

- [53] Hollaus, F., Diem, M., Sablatnig, R.: Binarization of multispectral document images. In: Proceedings 16th International Conference on Computer Analysis of Images and Patterns (CAIP 2015, Valletta, Malta), Part II, pp. 109–120 (2015). Springer
- [54] Diem, M., Hollaus, F., Sablatnig, R.: Msio: Multispectral document image binarization. In: 12th IAPR Workshop on Document Analysis Systems (DAS), pp. 84–89 (2016). IEEE
- [55] Hollaus, F., Diem, M., Sablatnig, R.: Multispectral image binarization using GMMs. In: 16th International Conference on Frontiers in Handwriting Recognition (ICFHR), pp. 570–575 (2018). IEEE
- [56] Zarai, Y., Lavee, T., Dershowitz, N., Wolf, L.: Integrating copies obtained from old and new preservation efforts. In: 12th International Conference on Document Analysis and Recognition, pp. 47–51 (2013). IEEE
- [57] Ronneberger, O., Fischer, P., Brox, T.: U-Net: Convolutional networks for biomedical image segmentation. In: Proceedings 18th International Conference on Medical Image Computing and Computer-Assisted Intervention (MICCAI 2015, Munich, Germany), Part III, pp. 234–241 (2015). Springer
- [58] Israel Antiquities Authority: Leon Levy Dead Sea Scrolls Digital Library. <https://www.deadseascrolls.org.il>. Accessed: 2024-10-15
- [59] Oprescu, A., Rosengarten, O., Shor, P.: Multispectral imaging and the digitization of the Dead Sea Scrolls. In: Book and Paper Group Annual, vol. 37, pp. 71–76. American Institute for Conservation, Washington, D.C. (2018)
- [60] Avian Technologies: Avian Black-S Water-based, spray-on diffuse black coating. <https://aviantechnologies.com/product/avian-black-s>. Accessed: 2024-10-15
- [61] Brown-deVost, B., Kurar-Barakat, B., Dershowitz, N.: Segmenting Dead Sea Scroll fragments for a scientific image set. arXiv preprint arXiv:2406.15692 (2024)
- [62] Boykov, Y., Kolmogorov, V.: An experimental comparison of min-cut/max-flow algorithms for energy minimization in vision. *IEEE transactions on pattern analysis and machine intelligence* **26**(9), 1124–1137 (2004)
- [63] Hollaus, F., Brenner, S., Sablatnig, R.: CNN based binarization of multispectral document images. In: International Conference on Document Analysis and Recognition (ICDAR), pp. 533–538 (2019). IEEE
- [64] Hedjam, R., Nafchi, H.Z., Moghaddam, R.F., Kalacska, M., Cheriet, M.: ICDAR 2015 c contest on m multispectral text extraction (MS-TEx 2015). In: 13th International Conference on Document Analysis and Recognition (ICDAR), pp. 1181–1185 (2015). IEEE
- [65] Kiessling, B.: Kraken—An universal text recognizer for the humanities. In: ADHO, Éd., Actes de Digital Humanities Conference (2019)

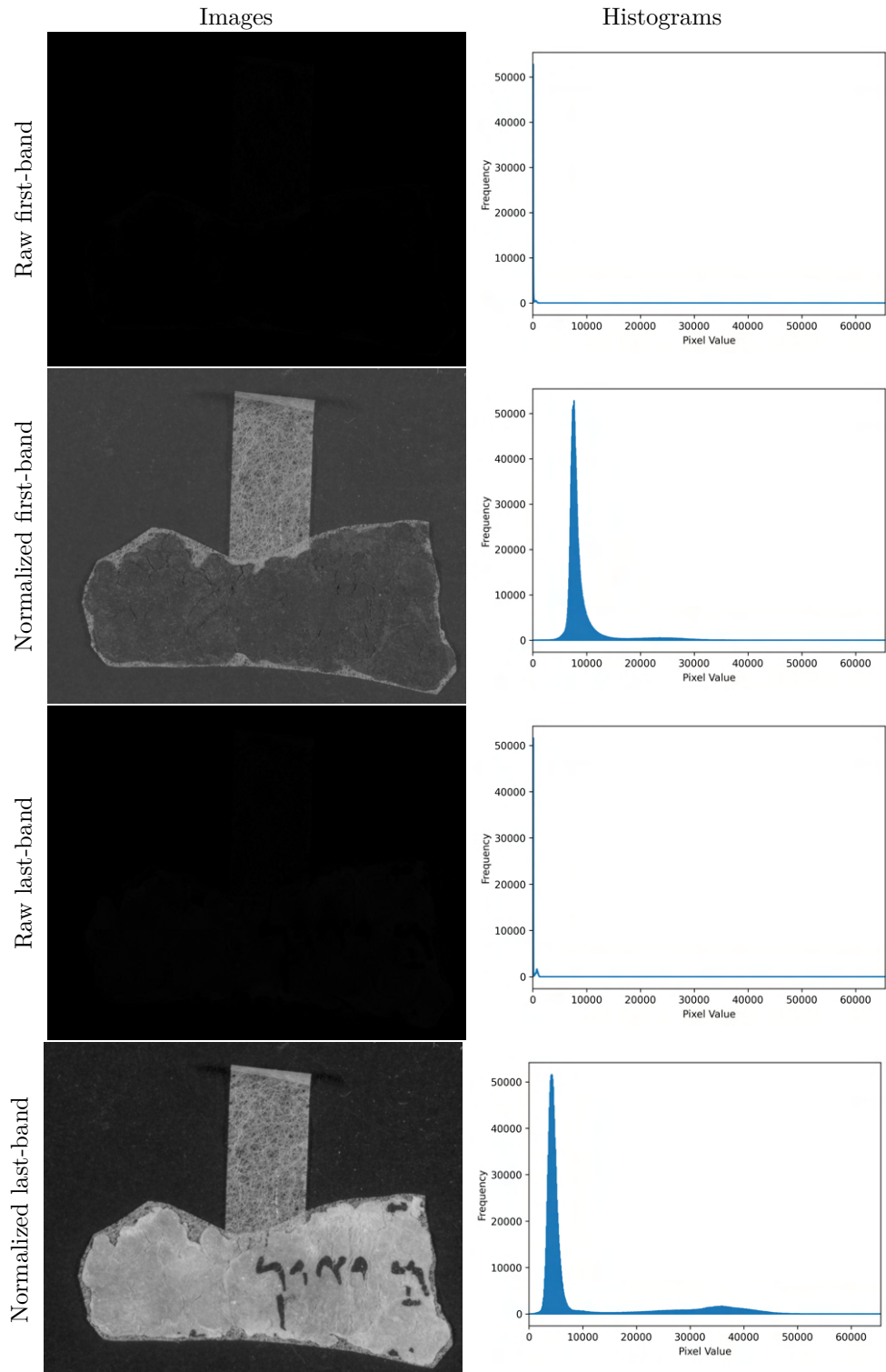


Fig. 22 The left column shows the raw 16-bit and normalized images for the first-band and last-band, while the right column displays their corresponding histograms. The raw images appear dark because the pixel values are concentrated in a narrow portion of the available range. Normalization expands these values, making features more visible and enhancing the overall contrast